418 *Macromolecules* **2010**, *43*, 418–427
DOI: 10.1021/ma9017795

Macromolecules
ARTICLE

Structural Rearrangements in a Lamellar Diblock Copolymer Thin Film during Treatment with Saturated Solvent Vapor

Zhenyu Di,[†] Dorthe Posselt,[‡] Detlef-M. Smilgies,[§] and Christine M. Papadakis*[,†]

[†]*Physikdepartment E13, Technische Universität München, James-Franck-Str. 1, 85747 Garching, Germany,* [‡]*IMFUFA, Department of Science, Systems and Models, Roskilde University, P.O. Box 260, 4000 Roskilde, Denmark, and* [§]*Cornell High Energy Synchrotron Source (CHESS), Wilson Laboratory, Cornell University, Ithaca, New York 14853*

Received August 8, 2009; Revised Manuscript Received October 30, 2009

ABSTRACT: We have investigated the structural changes in thin films of lamellar poly(styrene-*b*-butadiene) diblock copolymers during treatment with saturated cyclohexane vapor, a solvent slightly selective for polybutadiene. Using real-time, *in situ* grazing-incidence small-angle X-ray scattering (GISAXS), the swelling and the rearrangement of the lamellae were investigated with a time resolution of a few seconds, and the underlying processes on the molecular level were identified. After a few minutes in vapor, a transient state with higher degree of lamellar order and orientation was encountered. Additional parallel lamellae formed which we attribute to the increased degree of coiling of the polymers in the swollen state. Eventually, the film became disordered. These changes are attributed to the increased mobility of the swollen polymers, and the gradually decreasing segment−segment interaction parameter in the film as solvent is absorbed.

1. Introduction

Because of the repulsion between two chemically dissimilar blocks joined by a covalent bond, block copolymers have the ability to self-assemble into a rich variety of periodic patterns, which have repeat distances typically in the range of 10−100 nm.[1,2] Such nanostructures have the potential for a number of nanotechnology applications, e.g., ultrahigh-density data storage media,[3] molecular sieves,[4] dielectric reflectors,[5] and sensors.[6] In the bulk, the diblock copolymer morphology is controlled by the overall degree of polymerization, N, the volume fraction of one of the blocks, f, and the Flory−Huggins segment−segment interaction parameter χ between the two blocks. For thin films, confinement effects are important as well,[7] which are reflected in the interfacial tensions and additional entropic contributions to the free energy at the air−polymer and the polymer−substrate interface.[8−11] These parameters together with the roughness of the substrate[12] and the molar mass of the copolymer[13] determine the degree of preferential orientation of domains in the block copolymer film with regard to the substrate. However, the thin film preparation by solvent-casting or spin-coating does not necessarily lead to the equilibrium structure.[14,15] Often, only short-ranged order is observed in the self-assembled structures, which hampers many applications. Methods to bring the samples into their equilibrium states and to reduce the number of defects are thus highly desirable.

Several methods to equilibrate block copolymer films have been proposed: thermal annealing above the glass transition temperature (T_g),[13,16−18] electrical fields,[19−21] and solvent vapor treatment.[14,15,22−26] Thermal annealing is the most commonly used method because it is straightforward and efficient. By heating the block copolymer above the glass transition temperatures of the blocks, the chain mobility increases, and thermodynamic equilibrium can be achieved.[16] However, this process does not apply to all polymers. Some polymers have a T_g close to their thermal degradation temperature, whereas others cross-link during annealing at high temperature. Treatment with solvent vapor circumvents these problems and therefore attracts increasing interest.

Many groups have reported the improvement of long-range order *after* vapor treatment and subsequent drying. For instance, Kim et al. showed that vapor treatment of a thin film of cylinder-forming poly(styrene-*b*-ethylene oxide) with the common solvent benzene and subsequent drying resulted in highly oriented, nearly defect-free arrays of cylinders, which spanned the entire film thickness.[15] The same authors carried out vapor treatment on similar films and found that ion complexation of the PEO block enhances the long-range order upon solvent annealing.[26] The authors attributed this finding to the increase of the effective segmental interaction parameter χ between PS and PEO by the presence of the salt. Fukunaga et al. carried out vapor treatment of a terblock copolymer thin film using tetrahydrofuran, a common solvent for all three blocks.[24] The initial sponge-like morphology before vapor treatment transformed into lamellae after the vapor treatment, starting near the air−polymer interface and resulting in a multilayered structure throughout the film. Albalak et al. studied the structural changes of poly(styrene-*b*-butadiene-*b*-styrene) triblock copolymers after exposure to the vapor of hexane, methyl ethyl ketone, and toluene, respectively.[22] They observed an improvement of the long-range order and a complex behavior of the repeat distance as a function of vapor treatment time.

Despite extensive studies of resulting structures, the underlying molecular processes occurring during vapor treatment are still not well understood. It would be desirable to know which conditions—choice of solvent, vapor pressure, duration of treatment time, conditions of drying, etc.—are optimum for obtaining the desired structure. Moreover, apart from showing fundamentally interesting phenomena, a detailed understanding of the processes during

*Author for correspondence: e-mail Christine.papadakis@ph.tum.de; Fax +49-89-28912473.

 Published on Web 12/11/2009

restructuring is needed for the optimization of annealing procedures and for the design of sensors for volatile solvents, for instance.

Real-time grazing-incidence small-angle X-ray scattering (GISAXS) measurements allowed us to monitor the changes occurring *in situ* during solvent-induced swelling of a diblock copolymer thin film with a time resolution of a few seconds. In our previous studies, we performed vapor treatment of thermally annealed poly(styrene-*b*-butadiene) (P(S-*b*-B)) thin films having initially exclusively perpendicular or exclusively parallel lamellar orientation with respect to the substrate, and we used toluene, a good and nonselective solvent.[27,28] In thin films with initially perpendicular lamellae, the exposure to toluene vapor induced a transition from a 2D powder structure, i.e., lamellar domains with a preferential orientation perpendicular to the surface but randomly oriented within the film plane, to a more bulklike 3D powder, i.e., lamellar domains having all possible orientations, on a time scale as short as a few minutes.[27] In contrast, the exposure to toluene vapor of thin films with initially parallel lamellae resulted in a more complex behavior: An instability was observed during the first few minutes, i.e., the breakup of the existing lamellae and the formation of additional lamellae.[28] We attributed the latter findings to the tendency to more coiled molecular conformations upon solvent uptake. Since the more coiled block copolymers require a higher interfacial area, they can only be accommodated via the creation of additional lamellae, which results in a reorganization of the entire stack of lamellae. The appearance of a transient state on a time scale of a few minutes was previously unknown and indicates that thin film kinetics needs to be probed *in situ* and in real time.

In the present work, we used a thin lamellar P(S-b-B) film without thermal anneal in which, in contrast to the previously studied thermally annealed samples with somewhat different substrate properties, the lamellae were initially not well oriented. The sample is thus well-suited to follow the appearance of long-range order during vapor treatment. We carried out *in situ*, real-time GISAXS measurements during the exposure to saturated cyclohexane (CHX) vapor, which is slightly selective to polybutadiene (PB). Together with experiments using a solvent selective for PS,[29] we hope to get an understanding of the role of selectivity of the solvent. The paper is structured as follows: After the Experimental Section, we describe the structural study of the as-prepared thin diblock copolymer film. Then, we focus on the changes of the lamellar thickness, the film thickness, and the domain sizes during vapor treatment. Finally, we discuss the results in terms of the change in polymer mobility, the screening of the repulsive interaction between the two blocks by the solvent, and the change in chain conformation.

2. Experimental Section

2.1. Polymers. The poly(styrene-*b*-butadiene) (P(S-*b*-B)) diblock copolymer used in this study was synthesized by anionic polymerization.[30] Its molar mass is 22.1 kg/mol, which corresponds to a degree of polymerization $N = 374$, and it has a polydispersity index of 1.05.[31] The PB volume fraction is 0.49 ± 0.01. In bulk, the polymer forms lamellae with a lamellar thickness of 189 ± 1 Å, and the Flory−Huggins segment−segment interaction parameter is $\chi = A/T + B$, with $A = 21.6 \pm 2.1$ K and $B = -0.019 \pm 0.005$.[31] At room temperature, $\chi N = 20$; the sample is thus in the intermediate-segregation regime.[32] The order-to-disorder transition temperature (T_{ODT}) is 181 ± 2 °C, and the glass transition temperatures of the polystyrene (PS) and PB domains in the present copolymer are $T_g = 76$ and -89 °C, respectively, as measured by differential scanning calorimetry.[31]

2.2. Film Preparation. Thin films were prepared on UV-cleaned Si(100) wafers terminated with a native silicon oxide layer (Silchem Handelgesellschaft mbH). The pieces were 4 cm long and 2 cm wide. The contact angle of the wafers was 64.4° for water and 7.4° for toluene, as measured using a OCA 20 instrument (Dataphysics) together with the SCA20 measurement and analysis software. Using the Owens−Wendt and Kaelble method,[33,34] the surface energy was determined at 39.5 mN/m.

The polymers were dissolved at a concentration of 20 mg/mL in toluene, which is a good and close to nonselective solvent. The polymer solution was poured onto the Si wafers until these were completely wet, and films were spin-coated at 3000 rpm for 30 s and stored in vacuum at room temperature for 1 day to remove the residual solvent.

2.3. Atomic Force Microscopy (AFM). Tapping mode AFM experiments were carried out using an MFP 3D SA instrument (Asylum Research, Santa Barbara, CA), using point-probe silicon SPM sensors, type NSC35 (μMach) having a resonance frequency of 150 kHz. A set-point ratio of 0.8−0.9 was chosen. The average height of the terraces was determined from a height histogram over the entire area.

2.4. Grazing-Incidence Small-Angle X-ray Scattering (GISAXS). Scattering experiments were performed at beamline D1 at the Cornell High Energy Synchrotron Source (CHESS) at Cornell University in Ithaca, NY. The wavelength λ was 1.193 Å. The beam was 0.5 mm wide and 0.1 mm high. A CCD camera with a pixel size of 47.2 μm × 47.2 μm was used as a detector with a sample-to-detector distance of 1840 mm, resulting in a q-resolution of 1.35×10^{-4} Å^{-1}/pixel. $q_{\|} = (q_x^2 + q_y^2)^{1/2}$ and q_z are the in-plane and the normal components of the scattering vector, respectively. For small incidence and scattering angles, the coordinates of the 2D detector correspond approximately to q_y and to q_z, and we use this notation in the remainder of the paper. A tantalum rod (diameter 3 mm) was placed vertically in front of the CCD camera to shield it from the reflected beam as well as from the intense diffuse scattering at small q_y. However, the intense parasitic scattering of the specularly reflected beam prevented the use of longer measuring times. Thus, during vapor treatment, a strip of lead tape with a width of 5 mm was mounted in addition to the rod.

The lamellar orientation was determined from the GISAXS images as follows:[35] For lamellae having their interfaces parallel to the substrate surface, diffuse Bragg sheets (DBSs) are observed at q_z values[35]

$$q_z = k_{iz} + \sqrt{k_{cp}^2 + \left[\frac{2\pi m}{D_{\mathrm{lam}}^{\mathrm{par}}} \pm \sqrt{k_{iz}^2 - k_{cp}^2}\right]^2} \qquad (1)$$

where $k_{iz} = k_0 \sin \alpha_i$ and $k_{cp} = k_0 \sin \alpha_{cp}$ with $k_0 = 2\pi/\lambda$. α_i is the incidence angle of the X-ray beam with respect to the film surface. α_{cp} is the critical angle of total external reflection of P(S-*b*-B), at the chosen wavelength, $\alpha_{cp} = 0.12°$. $D_{\mathrm{lam}}^{\mathrm{par}}$ is the lamellar thickness of the parallel lamellae, and m is the order of the reflection. In case of symmetric lamellae, m takes only odd values. For each value of m, two DBSs denoted "minus branch (M)" and "plus branch (P)" are expected, which correspond to scattering of the direct beam (M) and of the beam reflected from the substrate (P), respectively.[35]

In case of randomly oriented lamellae, rings of high intensity around the direct beam (diffuse Debye−Scherrer rings, DDSRs) and around the specularly reflected beam are expected.[13] In contrast to transmission scattering, the intensity along the DDSR is not homogeneously distributed but is maximum near the Yoneda peaks appearing at the q_z values corresponding to the critical angles of the polymer film and the substrate and decays toward high q_z.[35] The lamellar thickness of the perpendicular lamellae, $D_{\mathrm{lam}}^{\mathrm{perp}}$, is calculated using Bragg's law

$$D_{\mathrm{lam}}^{\mathrm{perp}} = \frac{2\pi}{q_y} \qquad (2)$$

where q_y is the radius of the DDSR centered at the specularly reflected beam. Since the DBSs and the DDSRs are in some

cases weak, their positions and radii cannot always be read off directly. Therefore, ellipses were drawn into the 2D images to fit the DDSRs. Their two half-axes were read off in the q_z and the q_y direction, giving D_{lam}^{par} and D_{lam}^{perp} (calculated using eqs 1 and 2, respectively). For the precise determination of the lamellar orientation and the lamellar thickness in the dry state, we carried out GISAXS measurements at several incidence angles α_i between 0.05° and 0.5°, thus allowing fitting to eq 1 for a range of k_{iz} values. For vapor treatment, $\alpha_i = 0.18°$ was chosen, which results in a beam footprint on the sample having a length of 32 mm, which is smaller than the sample size. α_i is larger than both α_{cp} and the critical angle of the Si substrate, $\alpha_{cS} = 0.17°$; thus, internal film structures can be detected. Moreover, at this incidence angle, the DBSs are well separated both from the specularly reflected beam and the Yoneda peaks of the polymer and the substrate.

To determine the q_z position and the full width at the half-maximum along q_z of the DBS during vapor treatment, intensity profiles along q_z were created by averaging over the range $-0.0055\ \text{Å}^{-1} < q_y < 0.0055\ \text{Å}^{-1}$. The profiles were found to be fitted well by the following function:

$$I(q_z) = (q_z - q_{zS})^{-4} \frac{A}{\omega\sqrt{\pi/2}} \exp\left[-2\frac{(q_z - q_{z0})^2}{\omega^2}\right] + I_0 \qquad (3)$$

where q_{zS} is the q_z position of the specularly reflected beam, q_{z0} is the q_z position of DBS and $\omega = 0.849 \times$ fwhm, and I_0 is a constant background. The first term is a combination of a Gaussian describing the peak and the overall decay of the scattering intensity along q_z which follows the Fresnel transmission function.

Intensity profiles along q_y were created by averaging over the range $0.0308\ \text{Å}^{-1} < q_z < 0.0349\ \text{Å}^{-1}$, i.e., at the q_z value of the specularly reflected beam. These profiles comprise two peaks on a decaying background which could be modeled by a sum of two Lorentzians and a stretched Lorentzian:

$$I(q_y) = h_1 / \left[1 + 4\left(\frac{q_y - q_{y1}}{\omega_1}\right)^2\right] + h_2 / \left[1 + 4\left(\frac{q_y - q_{y2}}{\omega_2}\right)^2\right] + h_3 / \left[1 + 4\left(\frac{q_y}{\omega_3}\right)^3\right] \qquad (4)$$

The first two terms describe the peaks due to the P and M contribution of the first-order DDSR to the intensity profile, whereas the last term describes the decaying reflected beam. q_{y1} and q_{y2} are their position and ω_1 and ω_2 their fwhms. ω_3 is the width of the specularly reflected beam. h_1, h_2, and h_3 are the amplitudes. Here, we disregarded the complicated phase correlation between the three terms because the above equation was found to fit the curves well.

Interference of X-ray beams reflected at the air−polymer and the polymer−substrate interface results in additional intensity variations along q_z, i.e., waveguide resonances, which are especially pronounced between α_{cP} and α_{cS} with the exact locations in q_z being related to the film thickness.[36] In our system, these oscillations were most clearly seen as intensity modulations of the DDSR along q_z. Intensity profiles along q_z were obtained by averaging over the range $-0.035 < q_y < -0.030\ \text{Å}^{-1}$. The resulting waveguide resonance profiles were modeled using the IsGISAXS software,[37] treating the system as a homogeneous, flat film with the average index of refraction, $\delta = 2.0 \times 10^{-6}$, of PS and PB ($\delta_{PS} = 2.17 \times 10^{-6}$ and $\delta_{PB} = 1.88 \times 10^{-6}$, respectively). Varying the film thickness and the roughness, the period of the oscillations and the positions of the maxima were adjusted to match the experimental curves for each image. The resulting film thickness, D_{film}, was converted to the polymer volume fraction, $\phi = D_{film}^{dry}/D_{film}$, where D_{film}^{dry} and D_{film} are the film thicknesses in the dry state and during vapor treatment, respectively.

2.5. X-ray Reflectometry (XR). The film thickness was independently measured with XR. These experiments were carried out at CHESS beamline D1 using the collimating slits, goniometer, and sample environment of the GISAXS experiments. The detector was an ion chamber with an aperture of 50 mm height and 13 mm width mounted in front of the CCD camera. The direct beam spilling over the sample surface at low angles was blocked by a blade in front of the ion chamber. The measuring time was 1 s per point, and measuring the whole curve took ~10 min. The electronic background was measured and subtracted from the data. For fitting models of the scattering length density profiles normal to the sample surface, the software Parratt 32 (HMI Berlin) was used. In the fit, the scattering length density (SLD) of Si was fixed at $2.07 \times 10^{-5}\ \text{Å}^{-2}$. The SLD and thickness of the SiO_x layer were left as fitting parameters: an SLD value of $2.28 \times 10^{-5}\ \text{Å}^{-2}$ was obtained for both the as-prepared and the fully swollen film while thicknesses of 26 and 16 Å were obtained for the as-prepared and the fully swollen film, respectively. The decrease of thickness points to improved contact between polymer film and substrate. In the dry state, the SLD of the thin film was fixed at $8.99 \times 10^{-6}\ \text{Å}^{-2}$, which is the mean value of the SLDs of pure PS and PB (9.60×10^{-6} and $8.35 \times 10^{-6}\ \text{Å}^{-2}$, respectively). In the fully swollen state, $\phi \approx 0.55$, and the SLD of the thin film was fixed at $8.35 \times 10^{-6}\ \text{Å}^{-2}$, which complies with the volume weighted average of the SLD of the dry film and the solvent (8.99×10^{-6} and $7.56 \times 10^{-6}\ \text{Å}^{-2}$). To model the as-prepared film which has a rough surface, one top layer was added to the homogeneous part of the polymer film with large roughness and lower SLD than that of the polymer. This top layer corresponds to inhomogeneity of the film thickness. The fully swollen film was modeled adding two thin layers of higher and lower SLD to both the film surface and the film/substrate interface. One layer represents enrichment of PB at the film surface and the film/substrate interface, and the other adjacent layer represents a resulting PS-rich neighboring layer.

2.6. Vapor Treatment and Drying. *In situ* vapor treatment with CHX was performed using the sample cell shown in Figure 2 of ref 27. Its volume amounts to ~110 mL. Up to 3 mL of solvent can be injected remotely through a long Teflon capillary into the solvent reservoir at the bottom of the cell, i.e., ~2 cm below the sample. A time series was initiated such that 2−3 initial GISAXS images were taken before injection, and the time series continued during injection and subsequent solvent annealing. After 30 min, when the experiment was finished, there was still solvent present in the cell; i.e., the vapor pressure was close to saturation during the experiment.

A light bulb at the top of the cell heats the cell slightly and thus prevents condensation of solvent vapor on the sample and on the Kapton windows. In order to avoid beam damage of the polymer film, the sample was moved sideways after each exposure, such that a pristine spot was illuminated in each measurement. A second scan of the same region was started after 19 min. The results do not show any signs of beam damage from the first run. GISAXS images were recorded every 15 s (10 s for measurement and 5 s for CCD read-out, data storage, and change of sample position) for the first 19 min and every 25 s (extra 10 s waiting time) afterward. After 78 min of vapor treatment, the cell was opened and the film was left to dry.

3. Results

We first discuss the film structure in the dry state and then describe the structural changes when the sample is subject to CHX vapor.

3.1. Structure of the As-Prepared Film.

3.1.1. X-ray Reflectivity and Atomic Force Microscopy. The film thickness of the as-prepared sample was determined

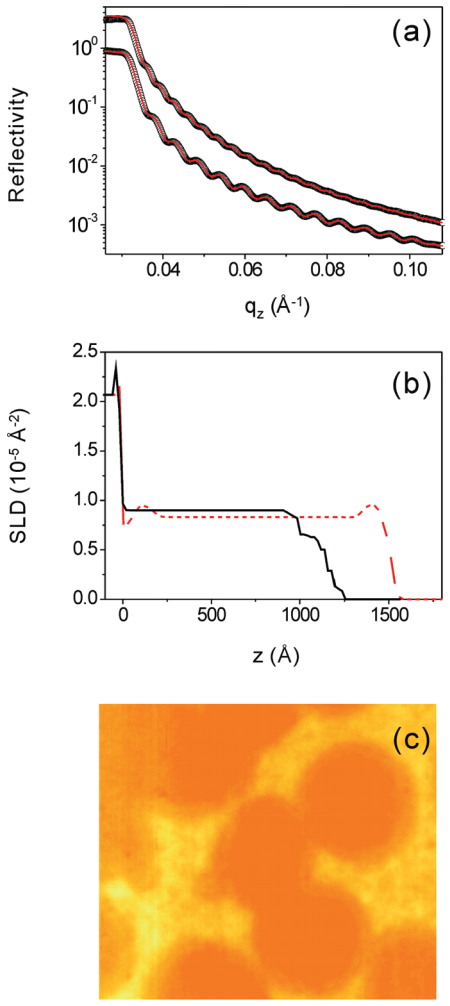

Figure 1. (a) XR curves of the as-prepared sample (lower curve) and the fully swollen film (upper curve). Symbols: experimental curves; lines: fitted model curves. (b) Models used to fit the XR curves. Black full line: as-prepared film; red dashed line: fully swollen film. The substrate surface is located at $z = 0$. (c) AFM height image of the as-prepared sample. Image size $5 \times 5\ \mu$m. The color scale runs from 45 nm (orange) to 75 nm (light yellow).

using XR. Figure 1a (lower curve) shows the measured XR curve together with a fit of a layer model which is shown in Figure 1b (black curve). The curve shows a number of Kiessig fringes. From modeling, the main part of the polymer film appears homogeneous with an SLD of 8.99×10^{-6} Å^{-2}, which is exactly the expected value of P(S-*b*-B). No inner layered structure is observed, which is consistent with the GISAXS results below. Only at the surface, a top layer (~180 Å) with a lower SLD is found. Such a layer may be attributed to the inhomogeneity of the film thickness after preparation or to terrace formation in the upper lamellar layer.[38] As shown below, the lamellar thickness in the thin film is $D_{\mathrm{lam}}^{\mathrm{par}} = 178 \pm 5$ Å, thus similar to the thickness of the top layer. The thickness of the homogeneous part of the film is 1016 ± 10 Å, which corresponds to $5.4 D_{\mathrm{lam}}$.

The terrace formation in the upper lamella could be confirmed by atomic force microscopy (Figure 1c). Terraces of an average height of 178 ± 30 Å are observed.

3.1.2. GISAXS. Figure 2 shows a 2D GISAXS image of the as-prepared film (measurement time 10 s). It features two DDSRs and a weak and broad DBS. A short-range ordered, microphase-separated morphology was thus present in the

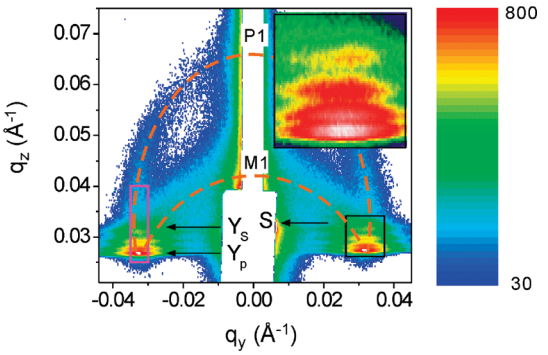

Figure 2. 2D GISAXS image of the as-prepared sample at $\alpha_i = 0.18°$. The measuring time was 10 s. The regions of low intensity (white rectangles in the center) are due to the rodlike beamstop and the lead tape. Arrows mark the positions expected for the Yoneda peaks of the polymer (Y_P) and the Si substrate (Y_S). The two ellipses indicate the two diffuse Debye−Scherrer rings, centered on the direct beam and the specularly reflected beam (marked "S"). M1 and P1 stand for the minus and the plus branch of the first-order DBS and DDSR (eq 1). The inset shows a zoom of the black rectangle. The left magenta box indicates the range of integration for the intensity profile in Figure 4.

film, i.e., lamellae having a broad distribution of orientations. The two DDSRs are due to scattering of the beam specularly reflected (upper ring, "P") from the substrate and scattering of the direct beam (lower ring, "M"). Because of dynamical effects, the rings are enhanced in the region between the Yoneda peak of the polymer and of the substrate. A certain fraction of the lamellae features a parallel orientation, as evident from the appearance of the DBS. The intensity of this DBS does not follow the general decline of the ring intensity toward high q_z.

We have previously observed that the P(S-*b*-B) diblock copolymer under study has a parallel lamellar structure in thermal equilibrium on Si wafers cleaned by detergent solution, water, and toluene.[13,17] In contrast, the present sample was spin-cast onto a UV-treated Si wafer. We conclude that the substrate properties and possibly details regarding the actual spin-coater used have an influence on the degree of lamellar orientation.

From the present single 2D GISAXS image, the lamellar thickness cannot be determined with high precision because the DBS is broadened along q_z and because the specularly reflected beam is shielded by lead tape. It becomes possible, though, using a series of GISAXS images taken at several values of α_i between 0.05° and 0.5° (Figure 3a−d). To precisely determine the position of the specularly reflected beam (which is a direct way for the exact determination of α_i), the lead tape was removed; thus, only shorter measuring times were possible, resulting in less good statistics. For $\alpha_i = 0.11°$, only very weak scattering is observed in the Yoneda band (Figure 3a). This incidence angle is below α_{cp}; thus, only scattering from a thin layer beneath the film surface can be observed.[39] The absence of scattering indicates that close to the film surface no pronounced, surface-induced structure is present. The images with α_i between α_{cp} and α_{cS} and slightly above (Figure 3b,c) show the same features as the image shown in Figure 2. For α_i significantly larger than α_{cS} (Figure 3d), the diffuse scattering is very weak because the reflectivity of the film/substrate interface is low.

Ellipses were constructed to the rings of diffuse scattering, and the lengths of their half-axes along q_z are given as a function of k_{iz} (i.e., α_i) together with the fitting curves (eq 1) in Figure 3e. The q_z values of the specularly reflected beam and of the Yoneda peaks from the polymer and the Si substrate are given as well. From the fits, we obtain

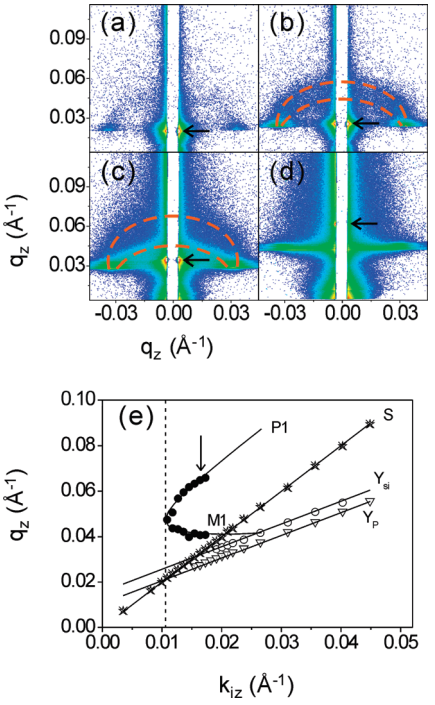

Figure 3. 2D GISAXS images of the as-prepared sample at $\alpha_i = 0.11°$ (a), 0.14° (b), 0.19° (c), and 0.34° (d). Measuring times were 0.3 s for (a−c) and 10 s for (d). The arrows indicate the position of the specularly reflected beam. The logarithmic intensity scale runs from 3 to 2000 cts for all images. (e) Resulting q_z positions of the specularly reflected beam (stars, marked S), the Yoneda peaks of the polymer (open triangles, Y_P), and the Si substrate (open circles, Y_S) as well as the q_z values of the DDSRs (filled circles) as a function of k_{iz} together with fits of eq 1 to the minus and the plus branch of the first order DDSR (marked M1 and P1, solid lines). The vertical dashed line marks the resulting k_{cP}. The arrow indicates the incidence angle used during vapor treatment.

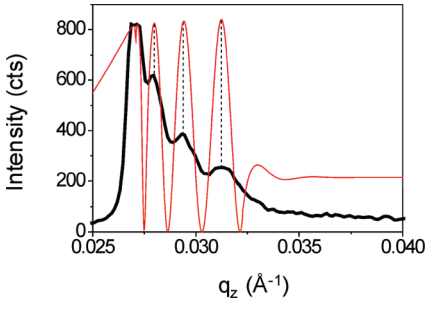

Figure 4. Black thick line: intensity profile along q_z through the DDSR of the as-prepared sample at $\alpha_i = 0.18°$. Red thin line: fit of the profile of a homogeneous, flat film; see text.

$D_{lam}^{par} = 178 \pm 5$ Å and $k_{cp} = 0.0105$ Å^{-1} (vertical dashed line), which corresponds to the mean value of k_{cp} for a symmetric blend of pure PS and pure PB. From the length of the q_y half-axes of the ellipses, the average D_{lam}^{perp} was found to be 188 ± 3 Å, i.e., the value is practically independent of α_i. D_{lam}^{perp} is thus equal to the bulk value (189 ± 1 Å). In contrast, D_{lam}^{par} is 6% lower than in the bulk. This effect has been previously observed by us.[17] The film thickness of the as-prepared sample and the thickness during swelling could be determined from the period of oscillations and the positions of the maxima in the intensity profiles along q_z through the DDSRs (Figures 2 and 4) as described in the Experimental Section. The positions of the maxima could be recovered very well. However, whereas in the model the amplitudes of the oscillations between the Yoneda peaks of the polymer film and the substrate are constant, the experimental curve decays with increasing q_z and shows less pronounced oscillations. We attribute this difference to the high roughness of the film surface (see XR result above) and to the presence of internal structure in the sample which is not included in the model. Fitting the position of the maxima, we obtain a film thickness of 970 ± 30 Å in the dry state (Figure 4), which agrees well with the value found by XR (1016 ± 10 Å). This fast method of film thickness determination from the GISAXS images was applied during vapor treatment, where XR measurements would take too long.

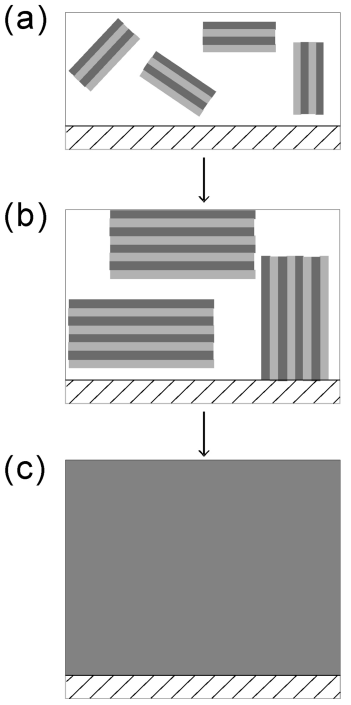

Figure 5. Sketch of the structure of the as-prepared sample (a), the transient state (b), and the final, disordered state (c). The different shades of gray indicate the PS and PB parts of the lamellae. For clarity, only a few lamellar domains are shown. The substrate is marked by dashes.

We conclude that, in the dry state, the film consists of domains of lamellae with short-range order and a wide distribution of orientations. A certain preference for the parallel lamellar orientation is found, as expected. D_{lam}^{perp} is very similar to the bulk value, whereas D_{lam}^{par} is 6% smaller than in the bulk. We summarize the structure of the as-prepared film in Figure 5a.

3.2. Structural Changes during Vapor Treatment. Cyclohexane (CHX) was used as the solvent for vapor treatment. It is known to be a good solvent for PB and a θ solvent for PS. It is thus slightly selective for PB, i.e., $\chi_{PB\text{-}CHX} < \chi_{PS\text{-}CHX}$. Therefore, the volume fraction of CHX in PB is expected to be slightly higher than in PS. Moreover, $\chi_{PB\text{-}CHX}$ and $\chi_{PS\text{-}CHX}$ both depend on ϕ.[38] The dependence is much weaker for $\chi_{PB\text{-}CHX}$ than for $\chi_{PS\text{-}CHX}$: $\chi_{PB\text{-}CHX}$ increases slightly from 0.26 to 0.36 for ϕ decreasing from 0.8 to 0, whereas $\chi_{PS\text{-}CHX}$ decreases from 0.92 to 0.51 in the same ϕ range. The values at $\phi = 0$ are calculated from the solubility parameters[41] and are consistent with the ϕ dependence. This means that during CHX vapor uptake, the selectivity of CHX varies. In the final state of swelling, where $\phi \approx 0.55$, the χ values are $\chi_{PS\text{-}CHX} \approx 0.8$ and $\chi_{PB\text{-}CHX} \approx 0.3$. For the poly(styrene-*b*-isoprene)/CHX system with $\chi_{PS\text{-}CHX} = 0.59$ and $\chi_{PI\text{-}CHX} = 0.39$, an uneven distribution with $\phi_{PS}^{CHX} = 0.71$ and $\phi_{PI}^{CHX} = 0.48$ was predicted (Figure 13a in ref 42.). In our case, the

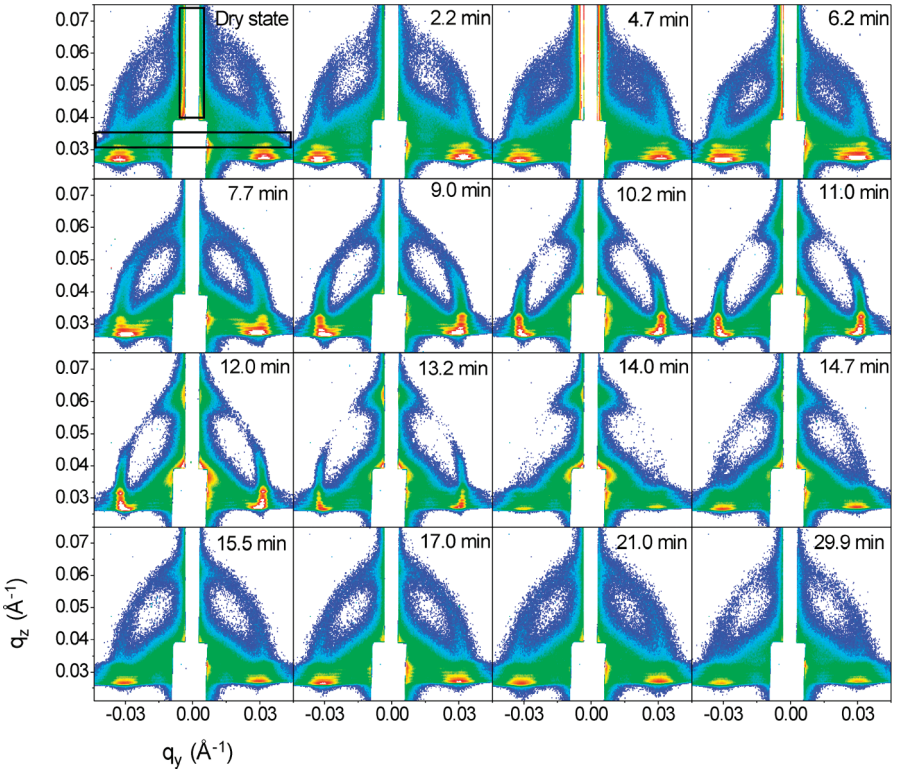

Figure 6. GISAXS images of the film during treatment with saturated CHX vapor for the times given in the figures. $\alpha_i = 0.18°$. The logarithmic intensity scale runs from 30 to 600 cts for all images. The boxes in the image of the dry state indicate the regions of integration used for obtaining the profiles along q_z (Figure 7a) and along q_y (Figure 7b).

selectivity, i.e., the difference of χ values, is higher throughout the entire experiment; thus, a more uneven distribution is expected. The values of the volume fraction of CHX in the PS and PB domains cannot, however, be calculated in a straightforward manner.

Upon injection of liquid CHX into the sample cell, drastic changes of the GISAXS images are observed (Figure 6): (i) During the first ~7.5 min, the radii of the DDSRs vary, while intensities and the DBSs are approximately unchanged. (ii) 7.5 to 13.5 min after injection, the DBSs get more pronounced and sharper, whereas the intensities of the DDSRs decrease drastically. (iii) After 13.5 min, the intensity along the DDSR reappears and becomes more evenly distributed. A transient state has thus been revealed. It is observed more clearly in the intensity profiles through the DDSRs and the DBSs (Figure 7): (i) For times shorter than 7.5 min, the profile through the DBS is flat (Figure 7a), and the profile through the DDSR shows a flat and broad peak at $q_y = 0.0323$ Å^{-1} (Figure 7b). We conclude that, in this time regime, the microphase-separated structure stays short-ranged (Figure 5a). (ii) Between 7.5 and 13.5 min, both profiles display well-pronounced peaks. This indicates the appearance of more long-ranged lamellar order (Figure 5b). (iii) For times longer than 13.5 min, the profile through the DDSRs display a weak and broad peak reminiscent of the correlation peaks observed in the disordered state,[31,32,43] and the DBSs disappear (Figure 5c). We will discuss the transition to the disordered state below.

In the following, we will quantify the thicknesses of the differently oriented lamellae, D_{lam}^{par} and D_{lam}^{perp} and compare these to the changes in the film thickness.

3.2.1. Lamellar Thicknesses. The lamellar thickness of the parallel lamellae, D_{lam}^{par}, is deduced from the q_z position of the DBSs. These can directly be read off from the peaks in the intensity profiles (Figure 7a) for vapor treatment times

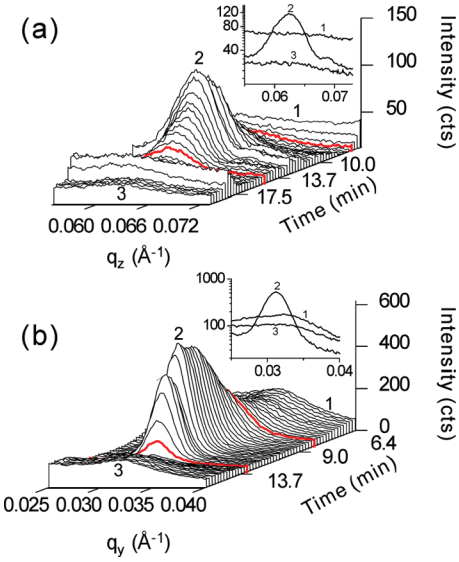

Figure 7. Intensity profiles along q_z, i.e., through the DBS (P1) (a), and along q_y, i.e., through the DDSR (P1) (b), from the images in Figure 6 as a function of treatment time. Representative profiles from the three time regimes marked 1−3 are shown in the insets. The thick red lines mark the times 7.5 and 15 min in (a) and 7.5 and 13.5 min in (b), i.e., when the peaks appear and vanish.

between 7.5 and 13.5 min. For earlier and later times, however, the DBSs are too weak to be fitted properly, and we therefore use the q_z intercept of the constructed ellipse. Good agreement was found between the two methods. The resulting q_z positions were converted to D_{lam}^{par} values using eq 1. For the perpendicular oriented lamellae, the positions of the peaks in the profiles shown in Figure 7b together with eq 2 were used to determine D_{lam}^{perp}. For simplicity, we use the

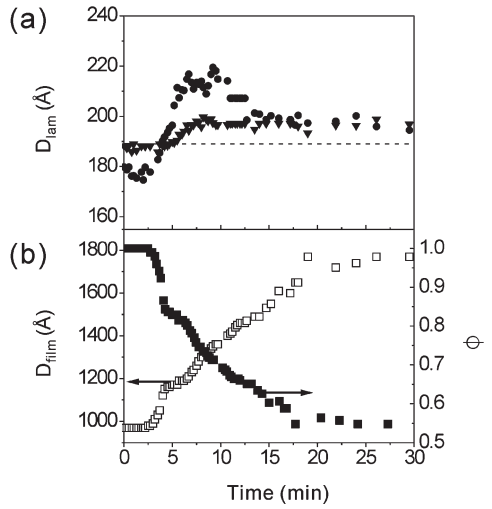

Figure 8. (a) D_{lam}^{par} (filled circles) and D_{lam}^{perp} (filled triangles) as a function of treatment time. The dashed line marks the bulk lamellar thickness.[31] (b) Film thickness as a function of treatment time (open squares, left axis) and the resulting volume fraction ϕ of P(S-*b*-B) in the swollen film (filled squares, right axis) as determined from the period of the waveguide oscillations in the GISAXS images.

term D_{lam} throughout, also in the disordered state after 13.5 min, where the value rather corresponds to the size of the correlation hole.[41] During the initial 13.5 min, D_{lam}^{par} and D_{lam}^{perp} show very different behavior as a function of treatment time (Figure 8a): During the first 5.3 min, D_{lam}^{perp} is unchanged at 188 Å. Then, D_{lam}^{perp} increases with a rate of 3.5 Å/min, i.e., by 1.9%/min, and reaches 197 Å after 6.5 min. Thereafter, the value stays constant. In contrast, the behavior of the parallel lamellae is more complex: During the first 2 min, $D_{lam}^{par} = 180$ Å; i.e., it is smaller than D_{lam}^{perp}. After 2 min, D_{lam}^{par} increases with a rate of 9.5 Å/min, i.e., by 5.3%/min, and reaches a plateau at 214 ± 5 Å after 6 min. The rate of swelling is thus higher than for the perpendicular lamellae. Then, D_{lam}^{par} decreases until it reaches 201 Å after 13.5 min. After this time, both values stay constant and are very similar to each other.

We conclude that both D_{lam}^{par} and D_{lam}^{perp} change during treatment with CHX vapor. Perpendicular lamellae are much more constrained laterally, and maybe this explains their slower thickness increase. The two types of lamellae differ in behavior during the first 15 min but then reach the same new equilibrium value. In the disordered state after 15 min, there is no more distinction between the two directions. We now relate the swelling behavior of the lamellae to the changes of the entire film, i.e., the overall solvent uptake.

3.2.2. Film Thickness. The film thickness as a function of vapor treatment time is determined from the period of the oscillations in the DDSR. The resulting film thickness, D_{film}, stays constant at 970 Å during the first 2 min (Figure 8b). Then, the film starts to swell at a rate of 42 Å/min, i.e., by 4.3%/min, until a new equilibrium value at 1780 Å is reached after 20 min. The rate of swelling is lower than the one of the parallel lamellae; i.e., the behavior is nonaffine. The final film thickness is 84% higher than in the dry state. The time-dependent volume fraction of polymer, $\phi = D_{film}^{dry}/D_{film}$, decreases from unity to 0.55 in the fully swollen state (Figure 8b).

During the first 2 min, no changes of the lamellar structure or film thickness are observed. The vapor of a good solvent is known to enter the polymer film not by type II diffusion with a sharp advancing boundary but via voids which are already present,[44,45] i.e., without a change of D_{film}. In our system, this kind of solvent uptake does not alter the lamellar thicknesses

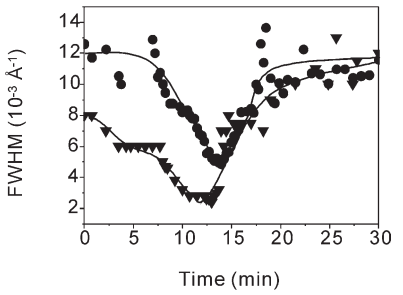

Figure 9. The fwhms of the DDSRs (P1) (filled triangles) and the DBSs (P1) (filled circles) as deduced from the peaks in Figure 7. The lines are guides to the eye.

either. From the voids, the solvent penetrates into the lamellar film, leading to an increase of D_{film} and to swelling of the two blocks.

3.2.3. Domain Sizes. To characterize the average domain size of the randomly oriented lamellae, we have determined the fwhms of the upper DDSR ellipse (P1) along q_y (Figures 7b and 9). During the first 7.5 min, the fwhms of the DDSR do not change significantly. Then, they decrease by a factor of ~2.8, and after 13.7 min, they increase rapidly and reach a constant value. The domain sizes of the perpendicular lamellae thus show a transient maximum.

The fwhms of the DBS along q_z reflect the average height of the correlated stack of parallel lamellae.[28] As shown in Figure 9, the domain sizes along q_z are similar to those along q_y and show the same behavior; i.e., also the domains consisting of parallel lamellae transiently contain a higher number of stacked lamellae. The minima in both domain sizes indicates a transient state of increased long-range order with domain sizes increased by a factor higher than 2.

3.3. Maximum Film Swelling. After 30 min of vapor treatment, the film appeared quasi-static, and we performed an *in situ* XR measurement for comparison (Figure 1a,b). We found that the film thickness had increased to 1530 Å with a roughness of 20 Å from initially 1016 Å with a roughness of 10 Å; i.e., the film thickness had increased by 50% due to solvent uptake. The polymer volume fraction, $\phi = D_{film}^{dry}/D_{film}$, has thus decreased to 0.66 ± 0.01. Using GISAXS, we determined the value 0.55 ± 0.02 from fitting the waveguide peaks in the Yoneda band. The difference in ϕ determined by XRR and GISAXS may be due to the difference in illuminated film area (different length of footprint). In the fully swollen state, at the film surface and at the film/substrate interface, indications of layering are observed with PB/CHX being preferentially adsorbed at both surfaces. The remainder of the film is homogeneous with an SLD of 8.35×10^{-6} Å^{-2}, which complies with the volume weighted average of PS, PB, and CHX (9.60×10^{-6}, 8.35×10^{-6}, and 7.56×10^{-6} Å^{-2} for PS, PB, and the solvent, respectively).

3.4. Structure after Drying. A GISAXS image was taken 10 min after the cell was opened (Figure 10). It shows that the ring of scattering is preserved, and thus the lamellae are randomly oriented. The intensity oscillations along q_z are still present; i.e., the film surface remains flat upon drying. The film thickness and the fwhm of the DDSR along q_y amount to 930 Å and 0.006 Å^{-1}, respectively, and are thus similar to the as-prepared sample. We conclude that the changes of the structure are reversible upon drying.

4. Discussion

Several interesting effects have been identified during swelling of the thin film with initially mixed lamellar orientation upon

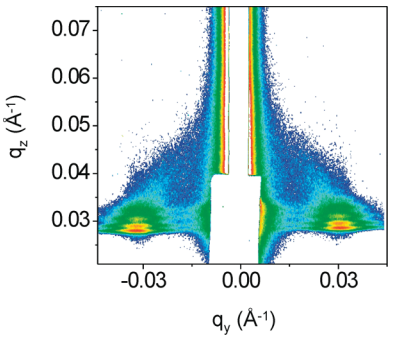

Figure 10. GISAXS image of the film after 78 min of treatment with saturated CHX vapor and 10 min of drying. $\alpha_i = 0.18°$. The logarithmic intensity scale runs from 30 to 600 cts.

treatment with cyclohexane, a slightly PB selective solvent: (i) Vapor treatment improves the lamellar order; the increased order, however, is lost again, resulting in a final disordered state. (ii) The swelling behavior of the parallel and the randomly oriented lamellae is different: Whereas the behavior of D_{lam}^{par} is characterized by an overshoot of 19% and a final value which is 12% higher than the one in the dry state, D_{lam}^{perp} increases after an incubation time of 5 min to the same final value as D_{lam}^{par} an overshoot. (iii) Comparison of D_{lam}^{par} and D_{film} shows that additional parallel lamellae are formed. For instance, after 13 min of treatment (just before the film disorders), $D_{film}/D_{lam}^{par} = 7.4$, which is significantly higher than in the dry state (5.4). This behavior is consistent with our previous observations on a lamellar P(S-*b*-B) film with initially parallel lamellae and treated with toluene.[28] (iv) The transient maxima of the domain sizes of the domains consisting of parallel and perpendicular lamellae reflect the transient state of improved long-range order before crossing the order-to-disorder transition. We will discuss these observations considering the effects of the uptake of CHX on P(S-*b*-B).

The uptake of CHX is expected to have several effects on the P(S-*b*-B) film: (i) The effective glass transition temperature T_g of the polymer blocks is decreased, which is especially important for the PS block (the T_g of PB is far below room temperature). As the PS glass transition is reached, the copolymer mobility increases, which enables large-scale structural rearrangements. (ii) The effective Flory−Huggins segment−segment interaction parameter between the two blocks, χ_{eff}, is reduced; thus, the enthalpic penalty for the creation of additional lamellar interfaces is decreased. (iii) In the presence of solvent, the copolymers assume more coiled molecular conformations than in the dry state where they are stretched away from the interface.[22,28,46] This implies an increased demand of interfacial area of each copolymer, thus promoting the formation of additional lamellae. In the following, we will discuss the resulting effect on the film structure.

4.1. Decrease of the Effective T_g. Following the Kelley−Bueche equation, the glass transition temperature T_g of a PS/CHX mixture in bulk varies with ϕ as[47]

$$T_{g,PS\text{-}CHX} = \frac{(1-\phi)\alpha_{CHX}T_{g,CHX} + \phi\alpha_{PS}T_{g,PS}}{(1-\phi)\alpha_{CHX} + \phi\alpha_{PS}} \qquad (5)$$

where α is the cubical thermal expansion coefficient of the fractional free volume, $\alpha_{CHX} = 1.23 \times 10^{-3}$ K^{-1},[48] $\alpha_{PS} \approx 1.9 \times 10^{-4}$ K^{-1},[49] and $T_{g,CHX} = 186$ K.[50] To estimate the variation of T_g, we assume for simplicity that CHX is equally distributed in PS and PB. This assumption of equal distribution only holds strictly for the later stages when the difference in $\chi_{PS\text{-}CHX}$ and $\chi_{PB\text{-}CHX}$ is small, whereas in the beginning of the treatment, CHX is slightly more PB selective as discussed above. The resulting $T_{g,PS\text{-}CHX}$ values during vapor treatment are given as a function of treatment time in Figure 11a. Already after 3.5 min of vapor treatment, $T_{g,PS\text{-}CHX}$ falls below room temperature. We expect the true glass transition at slightly later time than this estimate because CHX is not distributed evenly in the PS and PB domains, but in equilibrium PB is enriched in CHX.

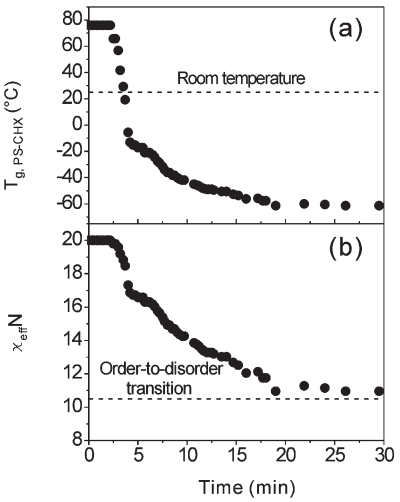

Figure 11. Effective T_g of the PS-rich domain (a) and $\chi_{eff}N$ (b) as a function of treatment time. The horizontal dashed lines in (a) and (b) indicate room temperature (25 °C) and the order-to-disorder transition.

The strong increase of the copolymer mobility thus promotes the feasibility of structural rearrangements after a few minutes of vapor treatment.

4.2. Decrease of χ_{eff}. The presence of solvent in the microphase-separated, lamellar morphology not only decreases T_g but also screens the repulsive interaction between the PS and the PB blocks. In the absence of solvent, $\chi N = 20$; the diblock copolymer melt is thus in the intermediate-segregation regime.[31] Starting from this low value, it is probable that χN reaches the value of 10.5 upon solvent uptake, where the order-to-disorder transition (ODT) is expected. For a nonselective solvent, χN of the copolymer is replaced by $\chi_{eff}N$ with $\chi_{eff} = \phi\chi$.[51] Using this assumption in spite of the slight selectivity of CHX, we find that $\chi_{eff}N$ of P(S-*b*-B) decreases with time as shown in Figure 11b during treatment with CHX vapor. After a treatment time of ~20 min, $\chi_{eff}N$ has decreased to 11; i.e., $(\chi N)_{ODT}$ is reached. Again, this time is only a crude estimate because the solvent distribution is presumably not equal in the PS and PB domain and because the exact value of $(\chi N)_{ODT}$ may be higher than 10.5 for a low molar mass copolymer, as stated by fluctuation theory.[52] However, it is striking that the ODT is reached significantly later than the glass transition. We assign the vanishing of the DBSs and DDSRs after 13.5 and 15 min, respectively, to the ODT of the copolymer in the presence of solvent. This small difference in time may indicate that the ODT is reached at lower ϕ for the perpendicular lamellae than for the parallel lamellae.

The transient state of increased lamellar order which persists in the time range 7.5−15 min is thus a result of the competition between the increased polymer mobility facilitating structural rearrangements and the order-to-disorder transition due to screening of the repulsive interaction between PS and PB. Conservation of the structure of the vapor-swollen film, e.g., by quick drying or chemical cross-linking, must be carried out during this transient state.

4.3. Increase of the Degree of Coiling. The behavior of the lamellar thickness of the parallel lamellae—overshoot and leveling off—resembles very much the one observed in our previous study where the initial morphology was purely

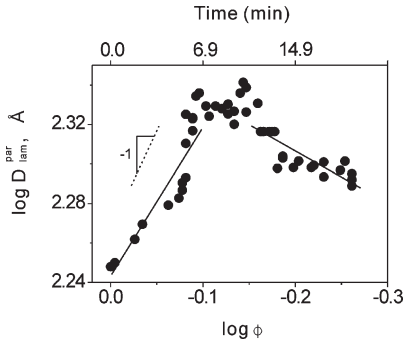

Figure 12. D_{lam}^{par} as a function of ϕ (lower axis) in a double-logarithmic representation. The time of vapor treatment is given on the top axis. The lines are fits of power laws; see text. The dashed line marks the predicted behavior $D_{lam}^{par} \propto \phi^{-1}$.

parallel and a nonselective solvent, toluene, was used.[28] However, the kinetics is different: In toluene vapor, the maximum of the overshoot was already reached after 3−4 min of treatment. The overshoot was attributed to predominantly uniaxial swelling with an unchanged interfacial area per chain in the first instant and the subsequent deswelling of the lamellae when the copolymers adopt a more coiled molecular conformation. The latter process only becomes possible when the polymers become mobile. It results in undulations of the lamellar interfaces and the creation of additional lamellae to allow more interfacial area per chain.

In the present work, we were able to compare the behavior of the parallel lamellae quantitatively to the mean-field predictions for the behavior of the lamellar thickness as presented in ref 53. Figure 12 shows the dependence of D_{lam}^{par} on ϕ. During vapor treatment, ϕ decreases from unity in the dry state to ~0.55 in the fully swollen state. In spite of the scatter in the data, two limiting regimes can be discerned: In the high-concentration regime (early times), an increase of D_{lam}^{par} following $D_{lam}^{par} \propto \phi^{-0.76\pm0.11}$ is observed. The swelling is thus slower than the uniaxial swelling predicted by mean-field theory, $D_{lam}^{par} \propto \phi^{-1}$, for the case that the interfacial area per chain is unchanged from the dry state.[53] The discrepancy may be due to the presence of randomly oriented lamellae. However, this swelling only lasts until $\phi = 0.81$ is reached, i.e., after ~6 min, when D_{lam}^{par} levels off. The glass transition of PS is reached, and the polymer becomes significantly more mobile, which enables the coiling of the copolymers and the formation of additional lamellae. In the low-concentration regime for $\phi < 0.72$, i.e., after ~8 min, $D_{lam}^{par} \propto \phi^{0.27\pm0.04}$. The latter behavior is in agreement with the mean-field prediction $D_{lam}^{par} \propto \phi^{1/3}$ (ref 53) and is related to the higher degree of molecular coiling in the presence of solvent. This coiling is only possible when the polymers are sufficiently mobile to move along and across the lamellar interfaces.

4.4. Behavior of Randomly Oriented Lamellae. The thickness of the perpendicular part of the randomly oriented lamellae stays constant during the first ~5.5 min, presumably because of the strong lateral constraints. Only after this time, the polymer is mobile enough for an increase of D_{lam}^{perp}. Eventually, D_{lam}^{perp} reaches the same value as the D_{lam}^{par}, consistent with a new equilibrium state, the disordered state, as argued above, has been reached at a polymer volume fraction of 0.55 in saturated CHX vapor. An ellipse was found to match the DDSRs well thoughout the vapor treatment. We thus conclude that the lamellae with intermediate orientation follow a behavior intermediate between the parallel and perpendicular ones.

5. Conclusions

Solvent vapor treatment offers an efficient route to control the structures in thin block copolymer films; however, the mechanisms are complex. In this paper, we report on the structural changes of a lamellar film which features a distribution of lamellar orientations before treatment. We observe that the orientation becomes more well-defined for a certain time, but then the film becomes disordered. Additional parallel lamellae are created during the process, which is consistent with our previous observation that the parallel orientation is the equilibrium one.[17,18] We relate the changes to the influence of solvent vapor on T_g and χN together with and the tendency to increased molecular coiling in the presence of solvent.

The time scale of the structural changes (< 30 min) is much lower than what has been reported in the literature for poly(styrene-*b*-methyl methacrylate) having a molar mass of 263 kg/mol.[25] Structural changes have been reported to occur during 120 h of treatment. The reason may be the ~10 times higher molar mass of the polymer and that the driving force of this system is mainly the change in surface energy by the solvent. In contrast, in our case, the film is thicker and the structural changes reflect rather the thermodynamics of the copolymer.

Using a thin film with several lamellae stacked allowed us to separate structural changes along the lamellar normal from those within the plane of the lamellar interface because of the macroscopic orientation of the lamellae along the film surface. Moreover, the vapor treatment of a thin film enabled us to address the low solvent concentration regime which is difficult with bulk samples. We were able to show that lamellar thin films of P(S-*b*-B) qualitatively follow the mean-field predictions at very low solvent concentration, $D_{lam}^{par} \propto \phi^{-0.76\pm0.11}$, whereas they quantitatively follow the predictions at higher solvent concentration, $D_{lam}^{par} \propto \phi^{0.27\pm0.04}$.

The different time scales observed in different systems for the appearance of more long-ranged order—between a few minutes and several days—seem to depend on a number of factors, such as the choice of the polymer and the solvent as well as the film thickness. The selectivity of the solvent for the soft PB domain slows down the kinetics.[28] A detailed understanding of the different factors is necessary for the controlled preparation of macroscopically ordered block copolymer films. In addition, the different kinetics of the structural changes when interacting with different solvents (selective, nonselective) might help in designing sensors for volatile solvents.

Acknowledgment. Financial support by the Graduate School of Excellence "Materials Science of Complex Interfaces" and DANSYNC/DANSCATT is gratefully acknowledged. CHESS is supported by NSF/NIH/NIGMS award DMR-0225180.

References and Notes

(1) Bates, F. S.; Fredrickson, G. H. *Annu. Rev. Phys. Chem.* **1990**, *41*, 525–557.
(2) Hamley, I. W. *The Physics of Block Copolymers*; Oxford University Press: Oxford, NY, 1998.
(3) Thurn-Albrecht, T.; Schotter, J.; Kästle, G. A.; Emley, N.; Shibauchi, T.; Krusin-Elbaum, L.; Guarini, K.; Black, C. T.; Tuominen, M. T.; Russell, T. P. *Science* **2000**, *290*, 2126–2129.
(4) Jin, C. Z.; Li, G.; Wang, X. S.; Zhao, L. X.; Liu, L. P.; Liu, H. O.; Liu, Y.; Zhang, W. P.; Han, X. W.; Bao, X. H. *Chem. Mater.* **2007**, *19*, 1664–1670.
(5) Urbas, A.; Fink, Y.; Thomas, E. L. *Macromolecules* **1999**, *32*, 4748–4750.
(6) Jung, Y. S.; Jung, W.; Tuller, H. L.; Ross, C. A. *Nano Lett.* **2008**, *8*, 3776–3780.
(7) Geisinger, T.; Müller, M.; Binder, K. *J. Chem. Phys.* **1999**, *111*, 5241–5250.

(8) Pickett, G. T.; Witten, T. A.; Nagel, S. R. *Macromolecules* **1993**, *26*, 3194–3199.
(9) Sommer, J. U.; Hoffmann, A.; Blumen, A. *J. Chem. Phys.* **1999**, *111*, 3728–3732.
(10) Potemkin, I. I. *Macromolecules* **2004**, *37*, 3505–3509.
(11) Potemkin, I. I.; Busch, P.; Smilgies, D.-M.; Posselt, D.; Papadakis, C. M. *Macromol. Rapid Commun.* **2007**, *28*, 579–584.
(12) Tsori, Y.; Sivaniah, E.; Andelman, D.; Hashimoto, T. *Macromolecules* **2005**, *38*, 7193–7196.
(13) Busch, P.; Posselt, D.; Smilgies, D.-M.; Rauscher, M.; Papadakis, C. M. *Macromolecules* **2007**, *40*, 630–640.
(14) Fukunaga, K.; Elbs, H.; Magerle, R.; Krausch, G. *Macromolecules* **2000**, *33*, 947–953.
(15) Kim, S. H.; Misner, M. J.; Xu, T.; Kimura, M.; Russell, T. P. *Adv. Mater.* **2004**, *16*, 226–231.
(16) Albalak, R. J.; Thomas, E. L.; Capel, M. S. *Polymer* **1997**, *38*, 3819–3825.
(17) Busch, P.; Posselt, D.; Smilgies, D.-M.; Rheinländer, B.; Kremer, F.; Papadakis, C. M. *Macromolecules* **2003**, *36*, 8717–8727.
(18) Sepe, A.; Di, Z.; Hoppe, T.; Magerl, D.; Perlich, J.; Darko, C.; Posselt, D.; Smilgies, D.-M.; Singh, M. A.; Papadakis, C. M., manuscript in preparation.
(19) Morkved, T. L.; Lu, M.; Urbas, A. M.; Ehrichs, E. E.; Jaeger, H. M.; Mansky, P.; Russell, T. P. *Science* **1996**, *273*, 931–933.
(20) Kyrylyuk, A. V.; Zvelindovsky, A. V.; Sevink, G. J. A.; Fraaije, J. G. E. M. *Macromolecules* **2002**, *35*, 1473–1476.
(21) Olszowka, V.; Hund, M.; Kuntermann, V.; Scherdel, S.; Tsarkova, L.; Böker, A.; Krausch, G. *Soft Matter* **2006**, *2*, 1089–1094.
(22) Albalak, R. J.; Capel, M. S.; Thomas, E. L. *Polymer* **1998**, *39*, 1647–1656.
(23) Elbs, H.; Fukunaga, K.; Stadler, R.; Sauer, G.; Magerle, R.; Krausch, G. *Macromolecules* **1999**, *32*, 1204–1211.
(24) Fukunaga, K.; Hashimoto, T.; Elbs, H.; Krausch, G. *Macromolecules* **2002**, *35*, 4406–4413.
(25) Xuan, Y.; Peng, J.; Cui, L.; Wang, H. F.; Li, B. Y.; Han, Y. C. *Macromolecules* **2004**, *37*, 7301–7307.
(26) Kim, S. H.; Misner, M. J.; Yang, L.; Gang, O.; Ocko, B. M.; Russell, T. P. *Macromolecules* **2006**, *39*, 8473–8479.
(27) Smilgies, D.-M.; Busch, P.; Papadakis, C. M.; Posselt, D. *Synchrotron Radiat. News* **2002**, *15*, 35–42.
(28) Papadakis, C. M.; Di, Z.; Posselt, D.; Smilgies, D.-M. *Langmuir* **2008**, *24*, 13815–13818.
(29) Di, Z.; Papadakis, C. M.; Posselt, D.; Smilgies, D.-M., to be published.
(30) Ndoni, S.; Papadakis, C. M.; Bates, F. S.; Almdal, K. *Rev. Sci. Instrum.* **1995**, *66*, 1090–1095.
(31) Papadakis, C. M.; Almdal, K.; Mortensen, K.; Posselt, D. *J. Phys. II* **1997**, *7*, 1829–1854.
(32) Papadakis, C. M.; Almdal, K.; Mortensen, K.; Posselt, D. *Europhys. Lett.* **1996**, *36*, 289–294.
(33) Owens, D. K.; Wendt, R. C. *J. Appl. Polym. Sci.* **1969**, *13*, 1741–1747.
(34) Kaelble, D. H.; Uy, K. C. *J. Adhes.* **1970**, *2*, 50.
(35) Busch, P.; Rauscher, M.; Smilgies, D.-M.; Posselt, D.; Papadakis, C. M. *J. Appl. Crystallogr.* **2006**, *39*, 433–442.
(36) Feng, Y. P.; Sinha, S. K.; Deckman, H. W.; Hastings, J. B.; Siddons, D. P. *Phys. Rev. Lett.* **1993**, *71*, 537–540.
(37) Lazzari, R. *J. Appl. Crystallogr.* **2002**, *35*, 406–421.
(38) Vignaud, G.; Gibaud, A.; Paris, F.; Ausserre, D.; Grübel, G. *Thin Solid Films* **1998**, *323*, 1–5.
(39) Tolan, M. *X-ray Scattering from Soft-Matter Thin Films: Materials Science and Basic Research*; Springer: Berlin, 1999.
(40) Krigbaum, W. R.; Geymer, D. O. *J. Am. Chem. Soc.* **1959**, *81*, 1859–1868.
(41) Grulke, E. A. In *Polymer Handbook*, 4th ed.; Brandrup, J., Immergut, E. H., Grulke, E. A., Eds.; Wiley: New York, 1999; Vol. *2*, p VII/678.
(42) Lodge, T. P.; Hamersky, M. W.; Hanley, K. J.; Huang, C. I. *Macromolecules* **1997**, *30*, 6139–6149.
(43) Leibler, L. *Macromolecules* **1980**, *13*, 1602–1617.
(44) Tang, Y.; Lu, J. R.; Lewis, A. J.; Vick, T. A.; Stratford, P. W. *Macromolecules* **2002**, *35*, 3955–3964.
(45) Müller-Buschbaum, P.; Bauer, E.; Maurer, E.; Cubitt, R. *Physica B* **2006**, *385*−*386*, 703–705.
(46) Shibayama, M.; Hashimoto, T.; Hasegawa, H.; Kawai, H. *Macromolecules* **1983**, *16*, 1427–1433.
(47) Kelley, F. N.; Bueche, F. *J. Polym. Sci.* **1961**, *50*, 549–556.
(48) Hartung, M.; Rauch, J.; Köhler, W. *J. Chem. Phys.* **2006**, *125*, 214904–214908.
(49) Schrader, D. In *Polymer Handbook*, 4th ed.; Brandrup, J., Immergut, E. H., Grulke, E. A., Eds.; Wiley: New York, 1999; Vol. *1*, p V/91.
(50) Prevosto, D.; Capaccioli, S.; Rolla, P. A.; Paluch, M.; Pawlus, S.; Hensel-Bielowka, S.; Kaminska, E. *J. Non-Cryst. Solids* **2006**, *352*, 4685–4689.
(51) Helfand, E.; Tagami, Y. *J. Chem. Phys.* **1972**, *56*, 3592–3601.
(52) Fredrickson, G. H.; Helfand, E. *J. Chem. Phys.* **1987**, *87*, 697–705.
(53) Noolandi, J.; Hong, K. M. *Ferroelectrics* **1980**, *30*, 117–123.